Intelligent Control Of An Electric Vehicle (ICEV)

Taoufik Chaouachi, Kamel Jemaï

Abstract: The electric vehicle allows fast, gentle, quiet and environmentally friendly movements in industrial and urban environments. The automotive industry has seen the opportunity to revive its production by replacing existing vehicles due to the reluctance of oil reserves around the world. In order to greatly reduce countries' dependence on oil, strategic sectors such as transport must increasingly integrate technologies based primarily on clean and renewable energy. Governments must implement large-scale measures to equip themselves with electric vehicles and build large recharge networks. The traditional system for conversions of conventional vehicles into electric vehicles consists of replacing the internal combustion engine and the gearbox with electrical components (engine and gearbox, or engine and gearbox), retaining the rest of the elements Transmission (transmission shafts, etc.).

Index Terms: Strategy of control, random perturbation method , fuzzy logic,power train vehicle,electric vehicle,Permanent magnetic synchronus motor.

1 INTRODUCTION

Reducing CO emissions represents a challenge for the transport sector. Transportation produces approximately 23 percent of the global CO emissions from fuel combustion. With rapid urbanization in developing countries, energy consumption and CO emissions by urban transport are increasing quickly[18]. Over the last few decades, the environmental impact of oil transport infrastructure, combined with the reluctance of energy resources, has led to renewed interest in an electric transport infrastructure. Electric vehicles differ from fossil fuel vehicles in that the electricity they consume can be produced from a wide range of sources, including fossil fuels, nuclear power and renewable Tidal energy, solar and wind energy or any combination of these. The energy consumption of these electric vehicles varies according to the fuel and the technologies used to produce electricity. Electricity can then be stored in the vehicle using an on-board battery[1], [5]. The electric motors are mechanically simple and often achieve high energy conversion efficiencies over the whole range of speed and power developed and can be controlled with high accuracy. They can also be combined with regenerative braking systems that have the ability to convert motion energy into stored electricity. This can be used to reduce brake system wear and reduce total energy consumption. Electric motors can be finely controlled and provide high starting torque, unlike internal combustion engines, and do not require multiple gears to match power curves. This eliminates the need for gearboxes and torque converters. Electric vehicles offer silent and smooth operation and therefore have less noise and vibration than internal combustion engines. In this work, we have incorporated new strategies for controlling the state variables of an electric vehicle based on fuzzy controllers. We attached particular importance to the mechanical transmission system by means of an appropriate modeling of the symbiosis between the electrical management system and the mechanical management system.

2 FUZZY STRATEGY

2.1 Fuzzy Studied Model

The topology of each fuzzy controller to integrate, was based on an interaction between two input variables, characterized successively by an error εxMi and an instantaneous variation of the error εxMi/$_{\partial t}$, to synthesize a fuzzy vector KxMi [6], [7],[8].

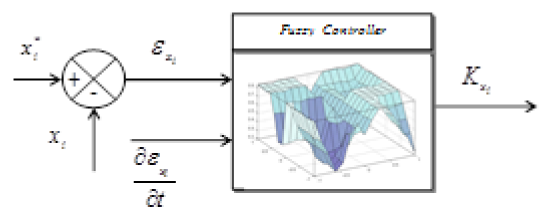

Fig.1.*Model of a fuzzy controller*

We defined the degree of membership of the error ε_{x_i} to a membership function $mfunc_r$ by $\mu^{\varepsilon_{x_i}}_{mfunc_r}$ and $\mu^{\frac{\partial \varepsilon_{x_i}}{\partial t}}_{mfunc_r}$ the degree of membership of the error variation to another membership function [18].

Let then:

$$\pi_{R_k} = \mu^{\varepsilon_{x_i}}_{mfunc_r} . \mu^{\frac{\partial \varepsilon_{x_i}}{\partial t}}_{mfunc_r} \quad (1)$$

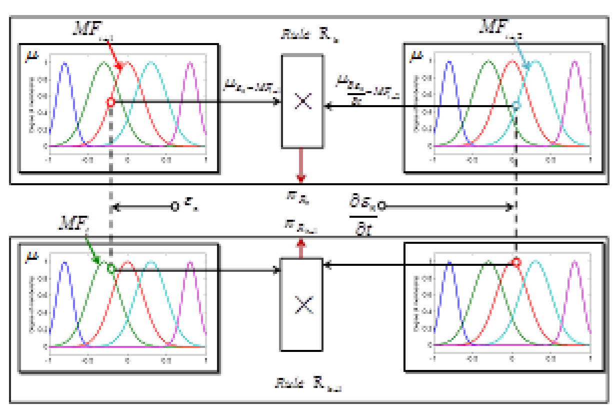

Fig.2. *Rulers treatment*

A surface S_{R_k} swept by the control vector for a rule R_k is given by: K_{x_i}

$$S_{R_k} = \pi_{R_k}.mfunc_r \qquad (2)$$

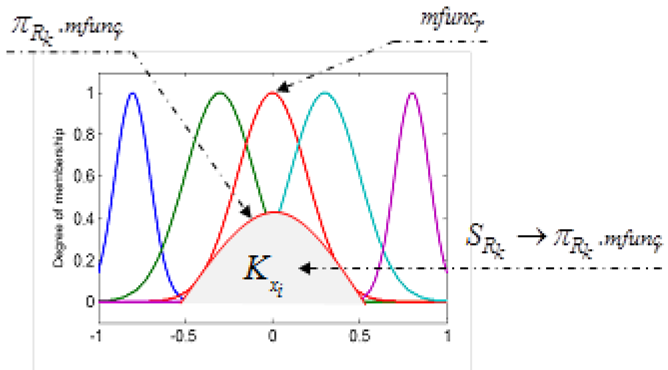

Fig.3.*Surface related to rule* R_k

Indeed, we have implemented a matrix of fuzzy inferences through a number of membership functions MF_i, Both for the error ε_x ($N_{\varepsilon_x} = 11$), That for its variation $\frac{\partial \varepsilon_x}{\partial t}$ ($N_{\frac{\partial \varepsilon_x}{\partial t}} = 11$) The same for the control vector U_f ($N_{U_f} = 11$), [15].

Thus, the total number of fuzzy inferences is given by :

$$N_{règles} = N_{\varepsilon_x}.N_{\frac{\partial \varepsilon_x}{\partial t}} = 121 \qquad (3)$$

These membership functions are specified in the following table:

Table 1 :
Membership functions

1	$MF_1 \Rightarrow MF_{NTG}$
2	$MF_2 \Rightarrow MF_{NG}$
3	$MF_3 \Rightarrow MF_N$
4	$MF_4 \Rightarrow MF_{NM}$
5	$MF_5 \Rightarrow MF_{NP}$
6	$MF_6 \Rightarrow MF_{ZE}$
7	$MF_7 \Rightarrow MF_{PP}$
8	$MF_8 \Rightarrow MF_{PM}$
9	$MF_9 \Rightarrow MF_P$
10	$MF_{10} \Rightarrow MF_{PG}$
11	$MF_{11} \Rightarrow MF_{PTG}$

where :
NTG: Negative Very Big,
NG : Negative Big,
N : Negative,
NM : Negative Medium ,
NP : Negative Small,
ZE : Zero,
PP : Positive Small ,
PM : Positif Medium,
P : Positif,
PG : Positif Big,
PTG : Positif Very Big.

The overall area swept by the fuzzy vector K_{x_i} after use of all the rules is formulated as follows :

$$S_{K_{x_i}} = \frac{\sum_{k}^{k=N_{R_k}} S_{R_k}}{N_{R_k}} \qquad (4)$$

With : N_{R_k} number of rules that are used. Thus, the fuzzy vector K_{x_i} is none other than the abscissa of the center of gravity of the overall surface $S_{K_{x_i}}$ swept by the control vector K_{x_i} and deduced in accordance with the relationship.

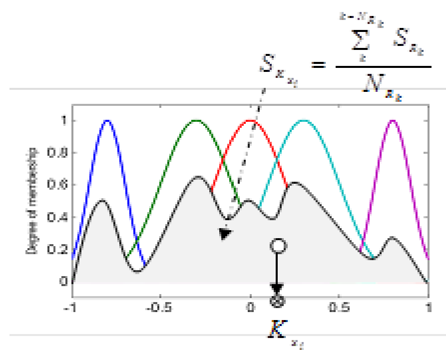

Fig.4. *Total surface swept by the fuzzy* control vector K_{x_i}

$$K_{x_i}^{nf} = \frac{\int_{-1}^{1} \pi_{R_k}.mfunc_r(K_{x_i}).K_{x_i}.\partial K_{x_i}}{\int_{-1}^{1} \pi_{R_k}.mfunc_r(K_{x_i}).\partial K_{x_i}} \qquad (5)$$

Where : $K_{x_i}^{nf}$ is an un-fuzzy vector.

2.2New Rescaling Technique

A new technique of scaling will be of great importance for the magnitudes of the state variables that may possibly exceed the extreme limits quoted. In other words, all sizes to be treated x_i giving rise to an error ε_{x_i} and a variation of error $\frac{\partial \varepsilon_{x_i}}{\partial t}$. Must undergo a transfer at the base of fuzzy variables evidenced by the interval [-1,1] , to generate the fuzzy input required for processing by the designated controller in accordance with the following system of equations [9]:

$$\begin{cases} \varepsilon_{x_i}^{f} = B_{\varepsilon}.\varepsilon_{x_i} + [1 - B_{\varepsilon}] \\ \frac{\partial \varepsilon_{x_i}^{f}}{\partial t} = B_{\frac{\partial \varepsilon}{\partial t}}.\frac{\partial \varepsilon_{x_i}}{\partial t} + [1 - B_{\frac{\partial \varepsilon}{\partial t}}] \\ B_{\varepsilon} = \frac{2}{G_{\max}^{ss}[mfunc_r(\varepsilon_{x_i})] - G_{\min}^{ss}[mfunc_r(\varepsilon_{x_i})]} \\ B_{\frac{\partial \varepsilon}{\partial t}} = \frac{2}{G_{\max}^{ss}[mfunc_r(\frac{\partial \varepsilon_{x_i}}{\partial t})] - G_{\min}^{ss}[mfunc_r(\frac{\partial \varepsilon_{x_i}}{\partial t})]} \end{cases} \quad (6)$$

Where:

$$\begin{cases} G_{max}^{ss}(mfunc_r(\varepsilon_{x_i})) = max\left\{\frac{1}{\sigma_{\varepsilon}.\sqrt{2.\pi}}.exp\left[-\frac{(\varepsilon_{x_i} - \mu_{\varepsilon})^2}{2.\sigma_{\varepsilon}^2}\right]\right\} \\ G_{min}^{ss}(mfunc_r(\varepsilon_{x_i})) = min\left\{\frac{1}{\sigma_{\varepsilon}.\sqrt{2.\pi}}.exp\left[-\frac{(\varepsilon_{x_i} - \mu_{\varepsilon})^2}{2.\sigma_{\varepsilon}^2}\right]\right\} \\ G_{max}^{ss}(mfunc_r(\frac{\partial \varepsilon_{x_i}}{\partial t})) = max\left\{\frac{1}{\sigma_{\partial\varepsilon}.\sqrt{2.\pi}}.exp\left[-\frac{(\frac{\partial \varepsilon_{x_i}}{\partial t} - \mu_{\partial\varepsilon})^2}{2.\sigma_{\partial\varepsilon}^2}\right]\right\} \\ G_{min}^{ss}(mfunc_r(\frac{\partial \varepsilon_{x_i}}{\partial t})) = min\left\{\frac{1}{\sigma_{\partial\varepsilon}.\sqrt{2.\pi}}.exp\left[-\frac{(\frac{\partial \varepsilon_{x_i}}{\partial t} - \mu_{\partial\varepsilon})^2}{2.\sigma_{\partial\varepsilon}^2}\right]\right\} \end{cases} \quad (7)$$

Where μ_i σ_i denote respectively the mean and standard deviation of the error and variation of error ε_{x_i} and $\frac{\partial \varepsilon_{x_i}}{\partial t}$. Similarly, the control vector K_{x_i} must undergo a transfer to the basic quantities studied, rescaled, to assign the value $K_{x_i}^{nf}$ and this means the system of equations:

$$\begin{cases} K_{x_i}^{nf} = B_{K_{x_i}^{nf}}.K_{x_i} + [1 - B_{K_{x_i}^{nf}}] \\ B_{K_{x_i}^{nf}} = \frac{G_{\max}^{ss}[mfunc_r(K_{x_i})] - G_{\min}^{ss}[mfunc_r(K_{x_i})]}{2} \end{cases} \quad (8)$$

Where:

$$\begin{cases} G_{max}^{ss}[mfunc_r(K_{x_i})] = max\left\{\frac{1}{\sigma_{K_{x_i}}.\sqrt{2.\pi}}.exp\left[-\frac{(K_{x_i} - \mu_{K_{x_i}})^2}{2.\sigma_{K_{x_i}}^2}\right]\right\} \\ G_{min}^{ss}[mfunc_r(K_{x_i})] = min\left\{\frac{1}{\sigma_{K_{x_i}}.\sqrt{2.\pi}}.exp\left[-\frac{(K_{x_i} - \mu_{K_{x_i}})^2}{2.\sigma_{K_{x_i}}^2}\right]\right\} \end{cases} \quad (9)$$

Through this new technique of rescaling, we assigned a dynamic behavior to the fuzzy controller in order to ensure better tracking of the variable to control [9].

3 ELECTRIC VEHICLE MODEL

The model of the electric vehicle studied is illustrated in figure 2. We focus mainly on the components of the power system that provide electric traction namely[11], [14]:

- The photovoltaic panel,
- The buck converter,
- The battery,
- The DC-Link,
- The DC/AC converter,
- The filter,
- The permanent magnet synchronous machine (PMSM).

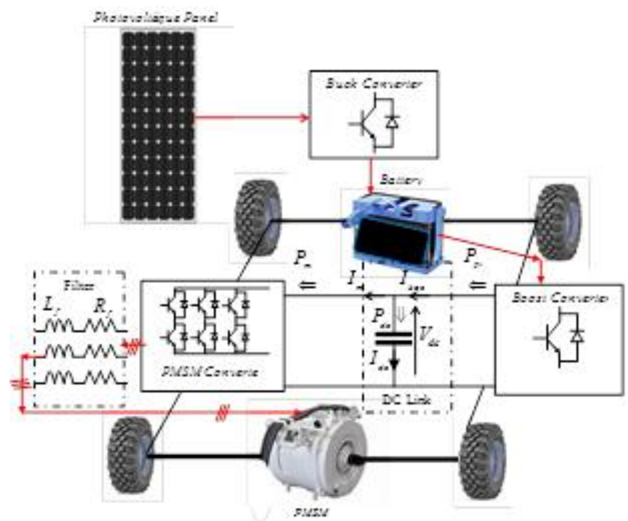

Fig.5. *Model of the studied electric vehicle*

4 PHOTOVOLTAIC GENERATOR

We start with a reminder of the electrical equations of the integrated photovoltaic generator. We highlight the model of the basic component of this generator, namely the photovoltaic cell with a real model.

4.1 Real Model of a Photovoltaic Cell

In order to highlight the physical phenomena that occur in the photovoltaic cell, we must consider:

- The leaks resulting from the edge effects of the junction PN and this by the integration of a shunt resistor R_{sh} in the equivalent scheme of the cell,
- The losses due to the contacts and the connections and which will be modeled, in the equivalent diagram, by a series resistance Rs.

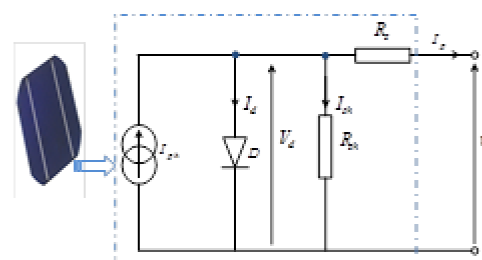

Fig.6. *Real modelof a photovoltaic cell*

The current supplied by the photovoltaic cell is then:

$$I_p = I_{ph} - I_s.\left[e^{\frac{V_p + R_s.I_p}{V_T}} - 1\right] - \frac{V_p + R_s.I_p}{R_{sh}} \quad (10)$$

The current I_{cc} supplied by the photovoltaic cell when the latter has a zero voltage to these terminals ($V_p = 0V$):

$$I_{cc} = I_{ph} - I_s.\left[e^{\frac{R_s.I_{cc}}{V_T}} - 1\right] - \frac{R_s.I_{cc}}{R_{sh}} \quad (11)$$

The voltage V_{co} delivered by the photovoltaic cell when the latter does not discharge any current ($I_p = 0A$) is:

$$V_{co} = V_T.Ln\left(\frac{I_{ph}}{I_s} - \frac{V_{co}}{R_{sh}.I_s} + 1\right) \quad (12)$$

The optimum power P_{op} delivered by the photovoltaic cell is defined when it delivers an optimum current I_{op} under an optimum voltage V_{op}:

$$P_{op} = V_{op}.I_{op} \quad (13)$$

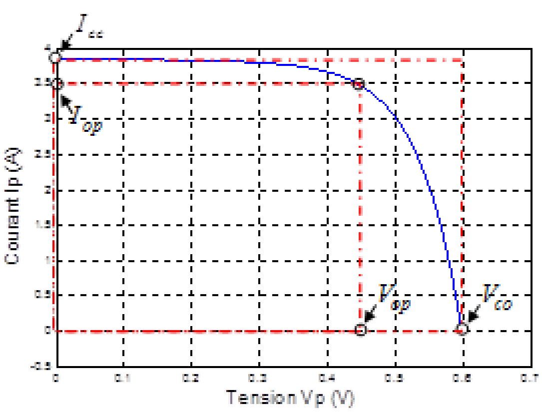

Fig.7. *Current voltage characteristic of a photovoltaic cell*

4.2 Model Of A Photovoltaic Generator

We present in the following the developed scheme of the model of a photovoltaic generator, figure 8.

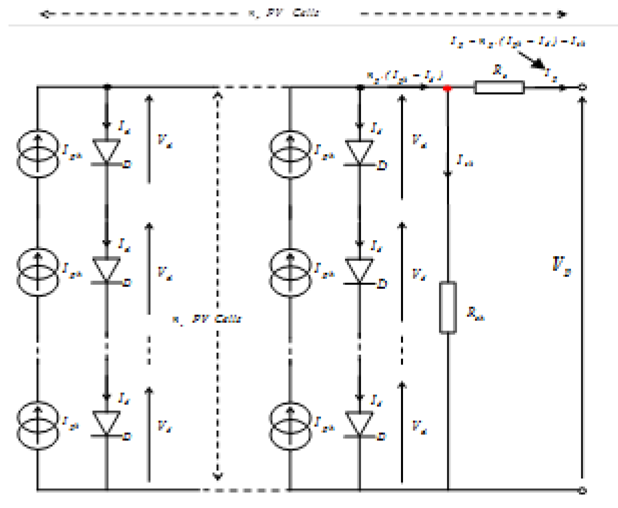

Fig.8. *Scheme of a photovoltaic generator*

The current supplied by the photovoltaic generator is expressed as follows:

$$I_p = n_p.I_{ph} - n_p.I_s.\left[e^{\frac{V_p + R_s.I_p}{n_s.V_T}} - 1\right] - \frac{V_p + R_s.I_p}{R_{sh}} \quad (14)$$

Taking into account that:

$$\begin{cases} R_s \to 0 \\ R_{sh} \to \infty \end{cases} \quad (15)$$

then:

$$I_p = n_p.I_{ph} - n_p.I_s.\left[e^{\frac{V_p + R_s.I_p}{n_s.V_T}} - 1\right] \quad (16)$$

The photovoltaic generator then delivers energy to the rest of the power circuit of the electric vehicle as shown in figure 9.

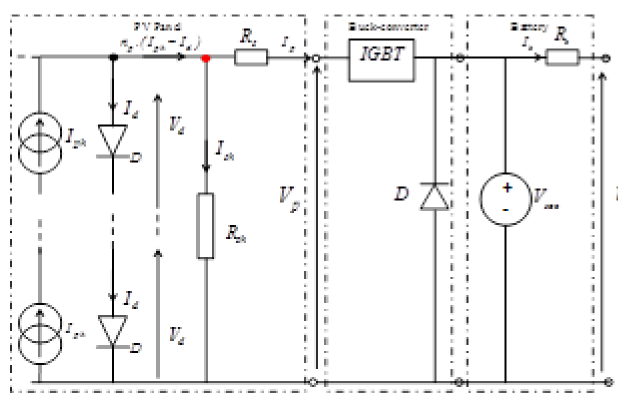

Fig.9. *Electric vehicle battery charging system*

5 Buck Converter

In order to ensure a conditioned transfer of the energy supplied by the photovoltaic generator (*Vp* , *Ip*) to the rest of the power system of the electric vehicle, we have integrated a buck converter. In fact, by checking the duty cycle α_{buc} of this converter, according to the requirement of the PMSM motor, we identify the level of the requested power of the photovoltaic (PV) generator. Let T_{buc} be the commutation cycle of the buck converter. From 0 to $\alpha_{buc}.T_{buc}$ we have:

$$V_p = L_{bu}.\frac{dI_p}{dt} + V_{soc} \qquad (17)$$

From $\alpha_{buc}.T_{buc}$ to T_{buc} we have:

$$0 = L_{bu}.\frac{dI_p}{dt} + V_{soc} \qquad (18)$$

And thus:

$$I_p = -\frac{V_{soc}}{L_{buc}}.(t - T_{buc}) + I_{p-min} \qquad (19)$$

On the other hand :

$$I_{p-max} = -\frac{V_{soc}}{L_{buc}}.(\alpha_{buc} - 1).T_{buc} + I_{p-min} \qquad (20)$$

The current I_p ripple noted ΔI_p is evaluated through the relationship:

$$\Delta I_p = I_{p-max} - I_{p-min} = \frac{1-\alpha_{buc}}{L_{buc}.f_{buc}}.V_{soc} \qquad (21)$$

Where :

$$f_{buc} = \frac{1}{T_{buc}}$$

Thus, we conclude that the average value of the voltage at the terminals of the storage battery V_{soc} is expressed as a function of the voltage applied by the photovoltaic generator V_p in accordance with the following relation:

$$\langle V_{soc} \rangle = \alpha_{buc}.V_p \qquad (22)$$

6 Battery Model

The charge separation that takes place in each battery cell give rise to a cell voltage, orOpen Circuit Voltage, OCV. As soon as the terminal ends are closed in an electrical circuit,chemical reactions start to take place in the cell, causing the flow of a current. However,due to the charge transport in the electrolyte, and the chemical reactions at the surfaceof the plates and the current in the plates, there is a resistance to the current, which iscalled the battery's internal resistance, R. A simple circuit model of a battery is depicted in Figure 10, where the OCV isdepending on the SOC, and the resistance is constant. There are, however, a number offactors that are not included in this simple model, such as the charge accumulation atthe plates, which gives capacitive contributions to the resistance, SOC and temperaturedependence of all parameters (OCV, R and C), and finally a self-discharge of the battery,that can be modeled as a shunt resistance to the OCV.

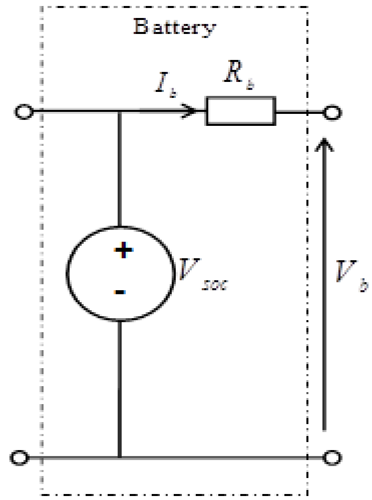

Fig.10. *Electric vehicle battery*

7 Boost Converter Model

The energy delivered by the storage battery (V_b, I_b)must meet the requirements imposed instantly, namely:

- Maintain a DC link voltage level V_{dc} required by the operating point of the PMSM motor,
- Determine the level of desired reference voltages (v^*_{dc}, v^*_{qc}) that the converter C_{PMSM} must supply.

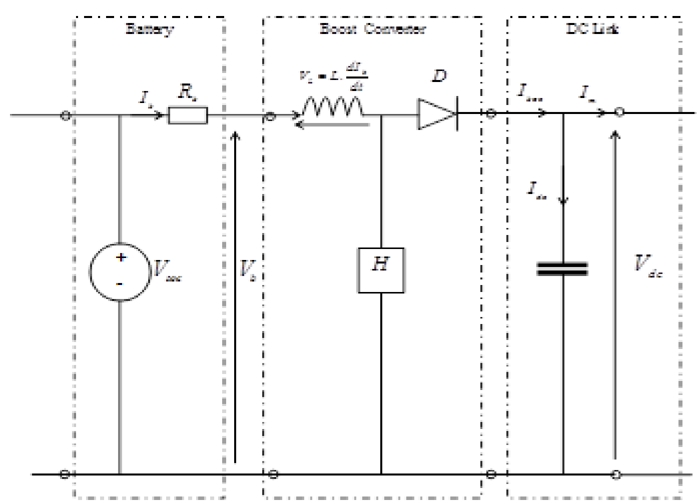

Fig.11. *Boost converter*

For these and other reasons, we have integrated a boost (step-up) converter with a duty cycle α_{boc} and a commutation cycle T_{boc}.

Referring to the figure 11, we write:

$$V_{dc} = \frac{1}{1-\alpha_{boc}}.V_b \qquad (23)$$

As already2 reported, Any operating point of the PMSM motor automatically imposes a DC-Link voltage level V_{dc} Therefore, we relied on the control of the duty cycle α_{boc}. For this purpose, a fuzzy controller evaluates an instantaneous reference of this duty cycle α^*_{boc} as a function of a desired level of the voltage reference level V^*_{dc}, figure 12.

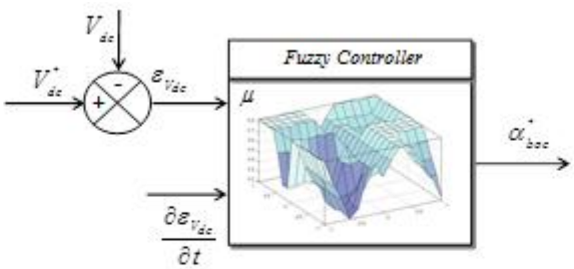

Fig.12. *Fuzzy control of the DC link voltage*

Referring to the above figure, the reference voltage V^*_b That the battery must supply is given by :

$$V^*_b = (1-\alpha^*_{boc}).V_{dc} \qquad (24)$$

Under these conditions, the level of the charge voltage V_{soc} of the battery is given by:

$$\begin{cases} V_{soc} = R_b.I_b + V^*_b \\ V_{soc} = \alpha_{buc}.V_p \end{cases} \qquad (25)$$

We thus go back in order to estimate the duty cycle α_{buc} of the buck converter as shown in figure 13, [15].

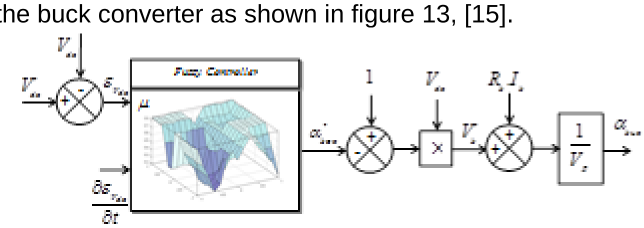

Fig.13. *Model of duty cycle α_{buc} control*

In figure 13, the DC-Link voltage level V_{dc} is evaluated by taking into account the transit powers P_{boc} and P_m :

$$V_{dc} = \sqrt{\frac{2}{C_{dc}}.\int_t^{t+pas}(P_{boc} - P_m).dt} \qquad (26)$$

Where pas is the step of calculation.

8 PERMANENT MAGNET SYNCHRONOUS MACHINE (PMSM) MODEL

The topology of the permanent magnet synchronous machine (PMSM) is illustrated in figure 14.By performing the transform Park to stator windings with respect to a reference associated with the rotor of the machine, we obtain a bipolar fictitious machine with axes (d,q),[14], [17].

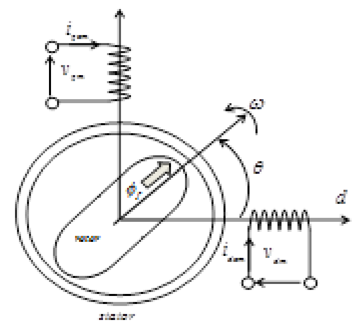

Fig.14. *Permanent magnet synchronous machine (PMSM) relating to (d, q) axes.*

The magnetic flux ϕ_f created by the permanent magnet at the rotor is oriented along the d-axis. Thus, the components of the voltage at the terminals of the stator of the PMSM machine are given by the following system:

$$\begin{cases} v_{dm} = R_s.i_{dcm} + \frac{d\phi_{dm}}{dt} - \omega.\phi_{qm} \\ v_{qm} = R_s.i_{qcm} + \frac{d\phi_{qm}}{dt} + \omega.\phi_{dm} \end{cases} \qquad (27)$$

The components of the fluxes along the (d,q) axes are given by the following system:

$$\begin{cases} \phi_{dm} = L_d.i_{dcm} + \phi_f \\ \phi_{qm} = L_q.i_{qcm} \end{cases} \qquad (28)$$

Taking into account the fluxes equations ϕ_{dm} and ϕ_{qm}, we write :

$$\begin{cases} v_{dm} = R_s.i_{dcm} + L_d.\frac{di_{dcm}}{dt} - \omega.L_q.i_{qcm} \\ v_{qm} = R_s.i_{qcm} + L_q.\frac{di_{qcm}}{dt} + \omega.(L_d.i_{dcm} + \phi_f) \end{cases} \qquad (29)$$

We then obtain two equivalent schemes along the (d,q) axes, figures 15 and 16.

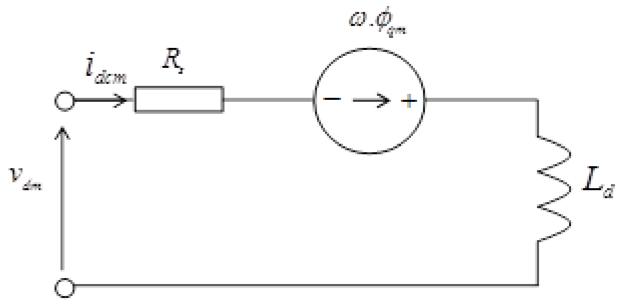

Figure 16 *Equivalent scheme of the PMSM machine according to the q-axis*

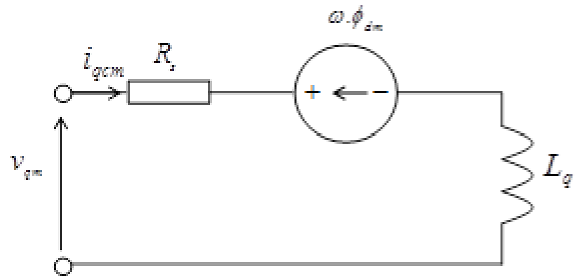

Fig.16.*Equivalent scheme of the PMSM machine according to the d-axis*

The active and reactive powers exchanged by the machine are:

$$\begin{cases} P_m = v_{dm}.i_{dcm} + v_{qm}.i_{qcm} \\ Q_m = v_{qm}.i_{dcm} - v_{dm}.i_{qcm} \end{cases} \quad (30)$$

We also write :

$$P_m = \frac{\Omega}{p}.(\phi_{dm}.i_{qcm} - \phi_{qm}.i_{dcm}) \quad (31)$$

Consequently, the electromagnetic torque T_{em} is then:

$$T_{em} = \frac{\phi_{dm}.i_{qcm} - \phi_{qm}.i_{dcm}}{p} \quad (32)$$

In order to plan the process of numerical integration of the equations of state of the PMSM machine and by referring to the system of equations (33), we write:

$$\begin{cases} \dfrac{di_{dcm}}{dt} = \dfrac{v_{dm} - R_s.i_{dcm} + \omega.L_q.i_{qcm}}{L_d} \\ \dfrac{di_{qcm}}{dt} = \dfrac{v_{qm} - R_s.i_{qcm} - \omega.(L_d.i_{dcm} + \phi_f)}{L_q} \end{cases} \quad (33)$$

On the other hand, the dynamics of the machine is described by the following model:

$$\begin{cases} \dfrac{d\omega}{dt} = \dfrac{T_{em} - T_r - \omega.f_r}{J_m} \\ \dfrac{d\theta}{dt} = \omega \end{cases} \quad (34)$$

Where : T_r Is the resistive torque, f_r coefficient of friction, J_m moment of inertia of the rotating mass and θ is the angular position. We have adopted the method of Runge Kutta of order 4 to evaluate the components of the current (i_{dcm}, i_{qcm}) Provided by the converter C_{PMSM} .

We write then:

$$\begin{cases} \dot{i}_{dcm} = \dfrac{v_{dm} - R_s.i_{dcm} + \omega.L_q.i_{qcm}}{L_d} = F_{dcm}(i_{dcm}, i_{qcm}, t) \\ \dot{i}_{qcm} = \dfrac{v_{qm} - R_s.i_{qcm} - \omega.(L_d.i_{dcm} + \phi_f)}{L_q} = F_{qcm}(i_{dcm}, i_{qcm}, t) \end{cases} \quad (35)$$

Therefore:

$$\begin{cases} i_{dcm}(n+1) = i_{dcm}(n) + \frac{1}{6}.pas.(rk_{dcm-1} + 2.rk_{dcm-2} + 2.rk_{dcm-3} + rk_{dcm-4}) \\ i_{qcm}(n+1) = i_{qcm}(n) + \frac{1}{6}.pas.(rk_{qcm-1} + 2.rk_{qcm-2} + 2.rk_{qcm-3} + rk_{qcm-4}) \end{cases} \quad (36)$$

With:

$$\begin{cases} rk_{dcm-1} = F_{dcm}(i_{dcm}, i_{qcm}, t) \\ rk_{dcm-2} = F_{dcm}(i_{dcm} + \frac{1}{2}.pas.rk_{dcm-1}, i_{qcm} + \frac{1}{2}.pas.rk_{qcm-1}, t + \frac{1}{2}.pas) \\ rk_{dcm-3} = F_{dcm}(i_{dcm} + \frac{1}{2}.pas.rk_{dcm-2}, i_{qcm} + \frac{1}{2}.pas.rk_{qcm-2}, t + \frac{1}{2}.pas) \\ rk_{dcm-4} = F_{dcm}(i_{dcm} + pas.rk_{dcm-2}, i_{qcm} + pas.rk_{qcm-2}, t + pas) \end{cases} \quad (37)$$

And:

$$\begin{cases} rk_{qcm-1} = F_{qcm}(i_{dcm}, i_{qcm}, t) \\ rk_{qcm-2} = F_{qcm}(i_{dcm} + \frac{1}{2}.pas.rk_{dcm-1}, i_{qcm} + \frac{1}{2}.pas.rk_{qcm-1}, t + \frac{1}{2}.pas) \\ rk_{qcm-3} = F_{qcm}(i_{dcm} + \frac{1}{2}.pas.rk_{dcm-2}, i_{qcm} + \frac{1}{2}.pas.rk_{qcm-2}, t + \frac{1}{2}.pas) \\ rk_{qcm-4} = F_{qcm}(i_{dcm} + pas.rk_{dcm-2}, i_{qcm} + pas.rk_{qcm-2}, t + pas) \end{cases} \quad (38)$$

9 Quadratic Control Of The DC Link Voltage Level

The level of the DC bus voltage is conditioned by the power balance ΔP_{dc} transited from the boost converter ΔP_{boc} to the C_{PMSM} converter ΔP_m ,we write then:

$$\Delta P_{dc} = \Delta P_{boc} - \Delta P_{m} \quad (39)$$

knowing that :

$$\begin{cases} P_{dc} = V_{dc}.I_{dc} \\ P_{boc} = \dfrac{1}{1-\alpha_{boc}}.V_b.I_{boc} \end{cases} \quad (40)$$

The fluctuations of the power P_{dc} are evaluated according to the following relation:

$$\Delta P_{dc} = \frac{\partial P_{dc}}{\partial V_{dc}}.\Delta V_{dc} + \frac{\partial P_{dc}}{\partial I_{dc}}.(\Delta I_{boc} - \Delta I_{m}) \quad (41)$$

We then find:

$$\Delta P_{dc} = \frac{\partial P_{dc}}{\partial V_{dc}}.\Delta V_{dc} + \frac{\partial P_{dc}}{\partial I_{dc}}.\Delta(I_{boc} - m_{cd}.i_{dcm} - m_{cq}.i_{qcm}) \quad (42)$$

Where m_{cd}, m_{cq} are the index modulations of the C_{PMSM} converter. The power involved in the DC bus is:

$$P_{dc} = \frac{1}{2}.C_{dc}.\frac{d(V_{dc}^2)}{dt} \quad (43)$$

then :

$$V_{dc}^2 = \frac{2}{C_{dc}}.\int_{t}^{t+pas} P_{dc}.dt \quad (44)$$

Which leads to:

$$V_{dc} = \sqrt{\frac{2}{C_{dc}}.\int_{t}^{t+pas}(P_{boc} - P_{m}).dt} \quad (45)$$

The notion of quadratic control comes from the fact that we treat the square of the DC bus voltage V_{dc}. Indeed, the control strategy is divided into two blocks namely a calculation block and a control block. In order to attribute to this strategy a better dynamic of pursuit of the desired reference V_{dc}^{*2}, we have opted for a fuzzy control, figure 17.

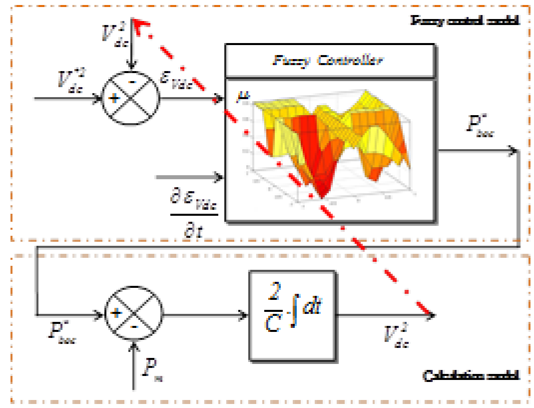

Fig.17. *Calculation and control models of the DC-link voltage*

10 SVPWM Strategy Applied To The *CPMSM* Converter

In this section, we are interested in developing the space vector pulse width modulation strategy (SVPWM) applied to the C_{PMSM} converter, figure 18.

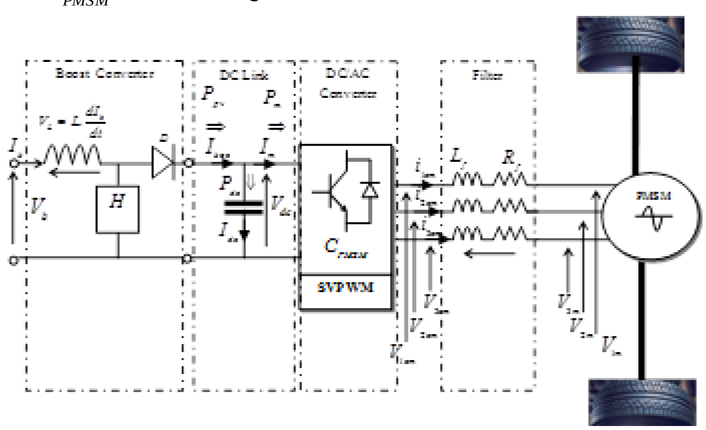

Fig.18. *model of the* C_{PMSM} *converter*

The output voltages of the C_{PMSM} converter are expressed as follow:

$$\begin{cases} v_{dcm} = R_f.i_{dcm} + L_f.\dfrac{di_{dcm}}{dt} - \omega.L_f.i_{qcm} + v_{dm} \\ v_{qcm} = R_f.i_{qcm} + L_f.\dfrac{di_{qcm}}{dt} + \omega.L_f.i_{dcm} + v_{qm} \end{cases} \quad (46)$$

R_f, L_f are respectively the resistance and the inductance of the filter.

We write likewise:

$$\begin{cases} v_{dcm} = m_{cd}.V_{dc} \\ v_{qcm} = m_{cq}.V_{dc} \end{cases} \quad (47)$$

Also :

$$\begin{cases} I_m = m_{cd}.i_{dcm} + m_{cq}.i_{qcm} \\ I_m = f_{cm}(i_{dcm}, i_{qcm}) \end{cases} \quad (48)$$

Current fluctuations ΔI_m at the input of the C_{PMSM} converter are written as follows:

$$\Delta I_m = \frac{v_{dcm}}{V_{dc}}.\Delta i_{dcm} + \frac{v_{qcm}}{V_{dc}}.\Delta i_{qcm} \quad (49)$$

Taking into account the Fortescue's theory based on decomposition into a positive synchronous reference frame (PSRF) and a negative synchronous reference frame (NSRF), figure 19, We implement control loops of currents and voltages.

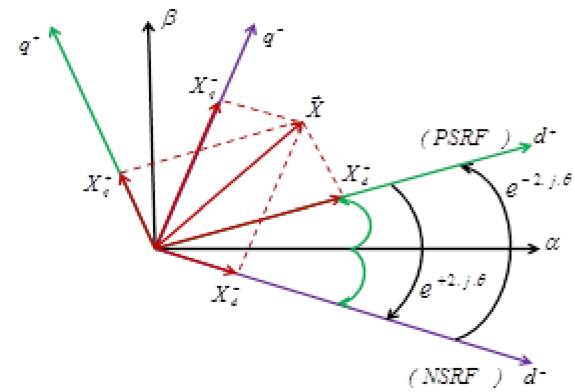

Fig.19.*Positive and a negative synchronous references frame (PSRF, NSRF)*

The current components (i_{dcm}, i_{qcm}) provided by the converter C_{PMSM} will be decomposed according to the following model.

$$\begin{cases} i_{dcm}^{+} = i_{dcmp}^{+} + i_{dcmn}^{-}.cos(2.\theta) + i_{qcmn}^{-}.sin(2.\theta) \\ i_{qcm}^{+} = i_{qcmp}^{+} + i_{qcmn}^{-}.cos(2.\theta) - i_{dcmn}^{-}.sin(2.\theta) \end{cases} \quad (50)$$

Where:

- x_d^{+}, x_q^{+} (d, q)-axiscomponents in the PSRF frame,
- x_{dp}^{+}, x_{qp}^{+} (d, q)-axiscomponents of the positive sequence in the PSRF frame,
- x_{dn}^{-}, x_{qn}^{-} (d, q)-axiscomponents of the negative sequence in the NSRF frame,

Thus, the fluctuations of the components of the current supplied to the machine are given by:

$$\begin{cases} \dfrac{\partial i_{dcm}^{+}}{\partial t} = -2.\omega.i_{dcmn}^{-}.\sin(2.\theta) + 2.\omega.i_{qcmn}^{-}.\cos(2.\theta) \\ \dfrac{\partial i_{qcm}^{+}}{\partial t} = -2.\omega.i_{qcmn}^{-}.\sin(2.\theta) - 2.\omega.i_{dcmn}^{-}.\cos(2.\theta) \end{cases} \quad (51)$$

The components of the reference voltage (v_{dm}^{*}, v_{qm}^{*}) applied to the terminals of the PMSM machine are evaluated in accordance with the following block diagram:

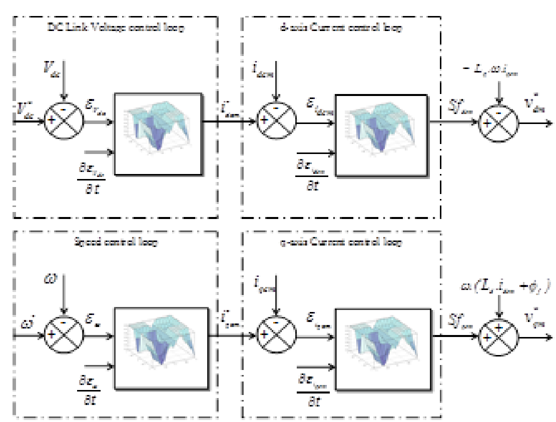

Fig.20. *Voltage control loops at the terminals of the PMSM machine*

We define the variations of the deviations $\varepsilon_{i_{dcm}}$, $\varepsilon_{i_{qcm}}$, ε_{ω} and $\varepsilon_{V_{dc}}$ by the following relations:

$$\begin{cases} \dfrac{\partial \varepsilon_{i_{dcm}}}{\partial t} = -2.\omega.i_{dcmn}^{-}.\sin(2.\theta) + 2.\omega.i_{qcmn}^{-}.\cos(2.\theta) \\ \dfrac{\partial \varepsilon_{i_{qcm}}}{\partial t} = -2.\omega.i_{qcmn}^{-}.\sin(2.\theta) - 2.\omega.i_{dcmn}^{-}.\cos(2.\theta) \\ \dfrac{\partial \varepsilon_{\omega}}{\partial t} = -\dfrac{T_{em} - T_r - \omega.f_r}{J_m} \\ \dfrac{\partial \varepsilon_{V_{dc}}}{\partial t} = -\dfrac{P_{dc}}{C_{dc}.V_{dc}} \end{cases} \quad (52)$$

The vectors Sf_{dcm} and Sf_{qcm} generated by the fuzzy controllers integrated in the (d, q) axis current control loops are defined as follows:

$$\begin{cases} Sf_{dcm} = R_s.i_{dcm} + L_d.\dfrac{di_{dcm}}{dt} \\ Sf_{qcm} = R_s.i_{qcm} + L_q.\dfrac{di_{qcm}}{dt} \end{cases} \quad (53)$$

The references of the components v^*_{dm} and v^*_{qm} of the voltage at the terminals of the PMSM machine being obtained and taking into account the existence of the (R_f, L_f) filter of the low-pass type,which completely eliminates all frequencies above the cutoff frequency while passing those below unchanged. We then constitute the components of the reference voltage v^*_{dc} and v^*_{qc} that the converter must generate:

$$\begin{cases} v^*_{dc} = R_f.i^*_{dc} - \omega.L_f.i^*_{qc} + v^*_{dm} \\ v^*_{qc} = R_f.i^*_{qc} + \omega.L_f.i^*_{dc} + v^*_{qm} \end{cases} \quad (54)$$

The components of the reference voltage v^*_{dc} and v^*_{qc} are subsequently transferred to a fixed reference frame (α, β) in order to apply the SVPWM technique.

$$\bar{v}^*_{\alpha\beta c} = e^{j.\omega.t}.\bar{v}^*_{dqc} \quad (55)$$

From where:

$$\begin{cases} v^*_{\alpha c} = \cos\theta.(R_f.i^*_{dc} - \omega.L_f.i^*_{qc} + v^*_{dm}) - \sin\theta.(R_f.i^*_{qc} + \omega.L_f.i^*_{dc} + v^*_{qm}) \\ v^*_{\beta c} = \sin\theta.(R_f.i^*_{dc} - \omega.L_f.i^*_{qc} + v^*_{dm}) + \cos\theta.(R_f.i^*_{qc} + \omega.L_f.i^*_{dc} + v^*_{qm}) \end{cases} \quad (56)$$

It is then necessary to locate the sector of belonging of the desired reference voltage vector $\bar{v}^*_{\alpha\beta c}$ which the C_{PMSM} converter must supply, figure 21.

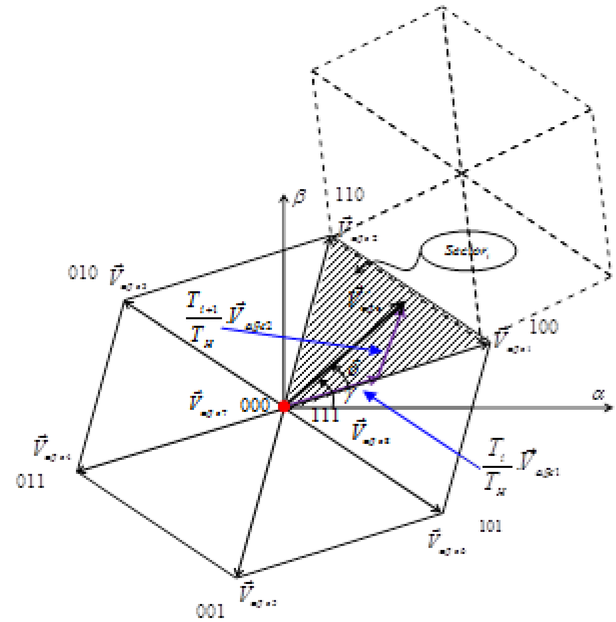

Fig.21. *SVPWM technic*

With referring to Figure 21, we write:

$$\begin{cases} \gamma = tan\,g^{-1}\left[\dfrac{\sin\theta.(R_f.i^*_{dc} - \omega.L_f.i^*_{qc} + v^*_{dm}) + \cos\theta.(R_f.i^*_{qc} + \omega.L_f.i^*_{dc} + v^*_{qm})}{\cos\theta.(R_f.i^*_{dc} - \omega.L_f.i^*_{qc} + v^*_{dm}) - \sin\theta.(R_f.i^*_{qc} + \omega.L_f.i^*_{dc} + v^*_{qm})}\right] \\ \delta = \gamma - angle(\bar{v}_{\alpha\beta 1}) \end{cases} \quad (57)$$

The distribution of the states of the keys $K_1K_2K_3$ as well as their application times T , over a modulation period T_H are illustrated in Figure 22.

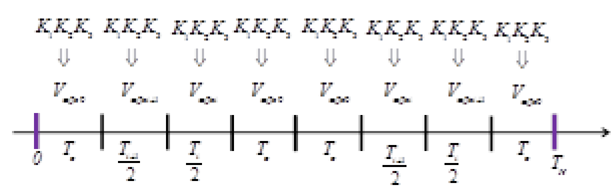

Fig.22. *Distribution of key control times*

The keys $K_1K_2K_3$ application times in a sector i are defined as follows:

$$\begin{cases} T_i = \sqrt{2}.\dfrac{v^*_{\alpha\beta c}}{V_{dc}}.T_H.sin[\,i.\dfrac{\pi}{3} - \gamma\,] \\ T_{i+1} = \sqrt{2}.\dfrac{v^*_{\alpha\beta c}}{V_{dc}}.T_H.sin[\,\gamma - (i-1).\dfrac{\pi}{3}\,] \end{cases} \quad (58)$$

Therefore, the average value of the voltage $\langle \bar{v}_{\alpha\beta c} \rangle$ supplied by the C_{PMSM} converter is:

$$\langle \bar{v}_{\alpha\beta c} \rangle = \frac{1}{T_H}.\left[T_0.\bar{v}_{\alpha\beta c0} + T_i.\sqrt{\frac{2}{3}}.V_{dc}.e^{j.(i-1).\frac{\pi}{3}} + T_{i+1}.\sqrt{\frac{2}{3}}.V_{dc}.e^{j.\frac{\pi}{3}} \right] \quad (59)$$

Where :

$$T_0 = \frac{T_H - T_i - T_{i+1}}{4} \quad (60)$$

This voltage will be transferred to the (d, q) reference frame according to the following relation:

$$\bar{v}_{dqc} = e^{-j.\theta}.\frac{1}{T_H}.\left[T_0.\bar{v}_{\alpha\beta c0} + T_i.\sqrt{\frac{2}{3}}.V_{dc}.e^{j.(i-1).\frac{\pi}{3}} + T_{i+1}.\sqrt{\frac{2}{3}}.V_{dc}.e^{j.\frac{\pi}{3}} \right] \quad (61)$$

11 Technique de Filtrage

In order to improve the quality of the energy exchanged between the C_{PMSM} converter and the PMSM machine, we have integrated a low pass filter (R_f, L_f). The filter cut-off frequency (f_c) is given by:

$$f_c = \frac{R_f}{2.\pi.L_f} \quad (62)$$

By application of the Laplace transform, the currents at the output of the (R_f, L_f)filter are expressed as follows:

$$\begin{cases} I_{dcm} = \dfrac{V_{dcm} - V_{dm} + \omega.L_f.I_{qcm}}{R_f + p.L_f} \\ I_{qcm} = \dfrac{V_{qcm} - V_{qm} - \omega.L_f.I_{dcm}}{R_f + p.L_f} \end{cases} \quad (63)$$

Numerically one writes:

$$\begin{cases} I_{dcm}(n) = \dfrac{L_f}{R_f.T_e + L_f}.I_{dcm}(n-1) + \dfrac{V_{dcm}(n) + \omega.L_f.I_{qcm}(n) - V_{dm}(n)}{R_f + \dfrac{L_f}{T_e}} \\ I_{qcm}(n) = \dfrac{L_f}{R_f.T_e + L_f}.I_{qcm}(n-1) + \dfrac{V_{qcm}(n) - \omega.L_f.I_{dcm}(n) - V_{qm}(n)}{R_f + \dfrac{L_f}{T_e}} \end{cases} \quad (64)$$

Or :

$$\begin{cases} I_{dcm}(n) = \dfrac{1}{2.\pi.f_c.T_e + 1}.I_{dcm}(n-1) + \dfrac{1}{L_f}.\dfrac{V_{dcm}(n) + \omega.L_f.I_{qcm}(n) - V_{dm}(n)}{2.\pi.f_c + \dfrac{1}{T_e}} \\ I_{qcm}(n) = \dfrac{1}{2.\pi.f_c.T_e + 1}.I_{qcm}(n-1) + \dfrac{1}{L_f}.\dfrac{V_{qcm}(n) - \omega.L_f.I_{dcm}(n) - V_{qm}(n)}{2.\pi.f_c + \dfrac{1}{T_e}} \end{cases} \quad (65)$$

Where T_e is the sampling period.

12 Phase Locked Loop (PLL)

The transformations of Park, by means of the use of the matrix $[P]$, Of axes (d, q) that we have established, Were based on arguments perfectly identical to those of the systems of voltages (currents) studied, (V_{ic}, I_{icm}).The aim of this approach was to reconstitute reference variables, assigned to the control loops, which were extremely precise, and on the other hand to aim at a perfect synchronization of the procedures for digital processing of the various state variables.

On the basis that:

$$\begin{cases} v_{dc} = \sqrt{\dfrac{3}{2}}.V_{c\,max}.cos(arg[P] - arg(v_{ic}(t))) \\ v_{qc} = -\sqrt{\dfrac{3}{2}}.V_{c\,max}.sin(arg[P] - arg(v_{ic}(t))) \end{cases} \quad (66)$$

In these circumstances, we must ensure that:

$$\arg[P] = \arg(v_{ic}(t)) \quad (67)$$

It then follows:

$$v_{qc} = -\sqrt{\frac{3}{2}}.V_{c\,max}.(arg[P] - arg(v_{ic}(t))) \quad (68)$$

Therefore, the phase locked loop (PLL) must guarantee the digital procedure established in figure 23.

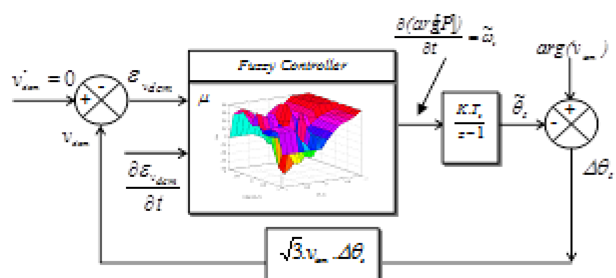

Fig.23. *Phase locked loop (PLL)*

13 Model of electric vehicle traction (EVT)

The model of the electric vehicle traction that emphasizes the different resistive torques T_{srm}, T_{srw}, T_w opposed to the electromagnetic torque T_{em} developed by the PMSM motor is illustrated in figure 24.

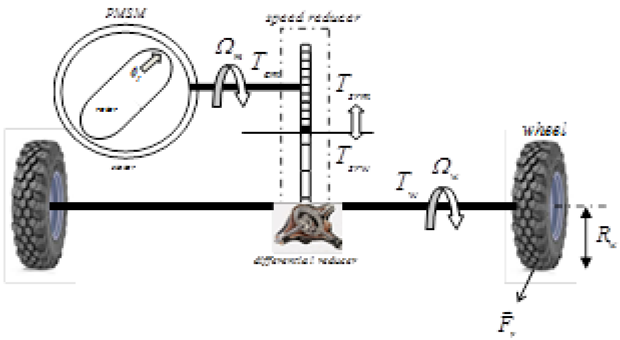

Fig.24.*Chain of traction*

Where:

- T_{srm} is the speed reducer torque of the PMSM side,
- T_{srw} is the speed reducer torque of the wheel side,
- T_w is the wheel torque.

In order to clarify the distribution of these different torques on the electric vehicle's shaft, we have used an analogy with the single-phase electric transformer, figure 25.

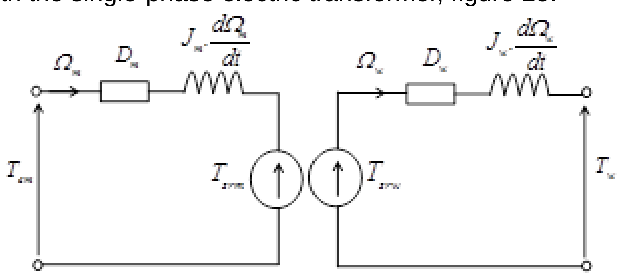

Fig.25. *Equivalent model of mechanical torque transfer*

By referring to the equivalent model of figure 25, we write:

$$\begin{cases} T_{em} = D_m.\Omega_m + J_m.\dfrac{d\Omega_m}{dt} + T_{srm} \\ T_{srw} = D_w.\Omega_w + J_w.\dfrac{d\Omega_w}{dt} + T_w \end{cases} \quad (69)$$

With:

$$\begin{cases} \Omega_w = r.\Omega_m \\ T_{srm} = r.T_{srw} \end{cases} \quad (70)$$

r Is the speed reduction ratio.

Then:

$$T_{em} = D_m.\Omega_m + J_m.\frac{d\Omega_m}{dt} + r.(D_w.r.\Omega_m + J_w.\frac{d(r.\Omega_m)}{dt} + T_w) \quad (71)$$

This leads to:

$$T_{em} = (D_m + r^2.D_w).\Omega_m + (J_m + r^2.J_w).\frac{d\Omega_m}{dt} + r.T_w \quad (72)$$

Finally:

$$T_{em} = D_{tm}.\Omega_m + J_{tm}.\frac{d\Omega_m}{dt} + r.T_w \quad (73)$$

where:

$$\begin{cases} D_{tm} = D_m + r^2.D_w \\ J_{tm} = J_m + r^2.J_w \end{cases} \quad (74)$$

The mechanical torque T_w applied to the wheel of the electric vehicle is given by the relation:

$$T_w = F_r.R_w \quad (75)$$

R_w The radius of the EV wheel.

F_r The resistive force (N),

On the other hand, the road and the quality of the coating have resistances external to the advance of the vehicle on a longitudinal plane. All the forces at the advancement can be represented by a single force of the second order: Under these conditions, the dynamics of the PMSM machine will be governed by the following mathematical model:

$$\begin{cases} \dfrac{d\Omega_m}{dt} = \dfrac{T_{em} - r.T_w - D_{tm}.\Omega_m}{J_{tm}} \\ \dfrac{d\theta_m}{dt} = \Omega_m \end{cases} \quad (76)$$

With:

$\Omega_m = \dfrac{\omega}{p}$, p is the number of pair poles.

14 The Forces Resisting Movement Of The Electric Vehicle

In order to evaluate with great precision the electromagnetic torque which the motor of the electric vehicle (EV) must develop, to overcome the total resisting force F_r opposed to the movement of the vehicle, we must establish the balance of all the forces $F_r = \sum_i F_{ri}$ likely to act during the movement of this vehicle. In effect, a moving vehicle is subjected overall to a force opposed to the penetration into the air F_{rap}, to a force of opposition to the rolling F_{rrol} and possibly to a force of opposition to the rise in a slope F_{rst} .

14.1 Force of penetration into air

This force F_{rap} is created by the mass of air that the vehicle in motion wishes to pass through.

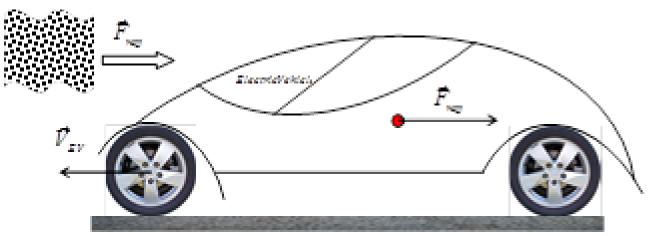

Fig.26. *Effect of the force of penetration into the air*

The force required to penetrate the air F_{rap}, it is calculated by applying the relation:

$$F_{rap} = \frac{1}{2}.\rho_{EV}.S.C_x.V_{EV}^2 \qquad (77)$$

Where :

ρ_{EV} The density of the vehicle,

S The surface taken to the wind,

C_x Coefficient of penetration into air,

V_{EV} Electric vehicle speed.

14.2 Rolling resistance force

This force F_{rrol} is applied to the vehicle as a result of the contact of these wheels with the road followed.

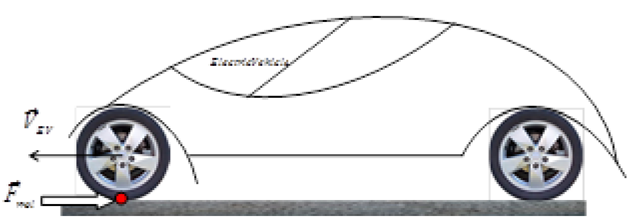

Fig.27. *Effect of the rolling resistance force*

The rolling resistance force F_{rrol} calculated by applying the relation:

$$F_{rrol} = M_{EV}.g.(k_{1rrol} + k_{2rrol}.V_{EV}^2) \qquad (78)$$

Where :

M_{EV} The mass of the vehicle,

g The acceleration of gravity,

k_{1rrol}, k_{2rrol} Coefficients of rolling resistance.

14.3 Slope force

This force F_{rst} is created at times when the vehicle attacks a slope. In fact, it depends on the weight of the vehicle P_{EV} and the angle of inclination of the road δ_p used by the vehicle.

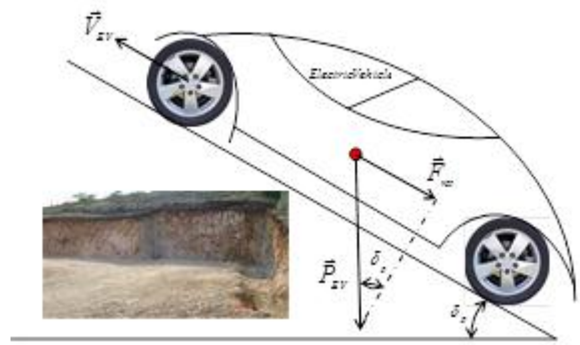

Fig.28. *Effect of the sloping terrain force*

The force to be defeated on a sloping terrain F_{rst} is calculated by mean of the following relation:

$$F_{rst} = P_{EV}.sin(\delta_p) \qquad (79)$$

Where $P_{EV} = M_{EV}.g$.

14.4Centrifugal Force

In Newtonian mechanics centrifugal force *Fc* is a force of inertia directed outside the axis of rotation which seems to act on all objects when they are observed in a rotating reference frame. The concept of centrifugal force can be applied to vehicles in rotational motion according to a certain curvature.

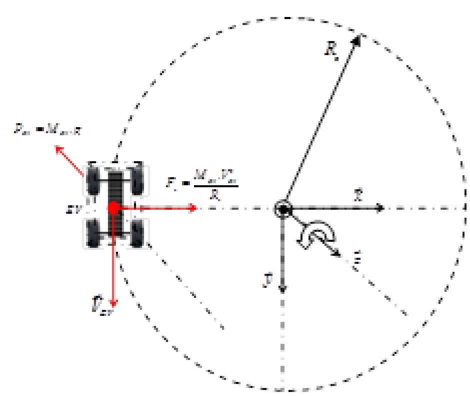

Fig.29. *Centrifugal force applied to anelectric vehicle*

Its intensity is given by the formula:

$$F_c = \frac{M_{EV}.V_{EV}^2}{R_c} \qquad (80)$$

Rc Is the distance from the axis of rotation to the center of gravity of the electric vehicle (EV), i.e. the radius of curvature of the path in meters (m).This reaction force *Fc* is sometimes described as a centrifugal inertial reaction [37] [38] that is a force which is centrifuged, which is an equal and opposite reactive force to the centripetal force which is the curvature of the path.

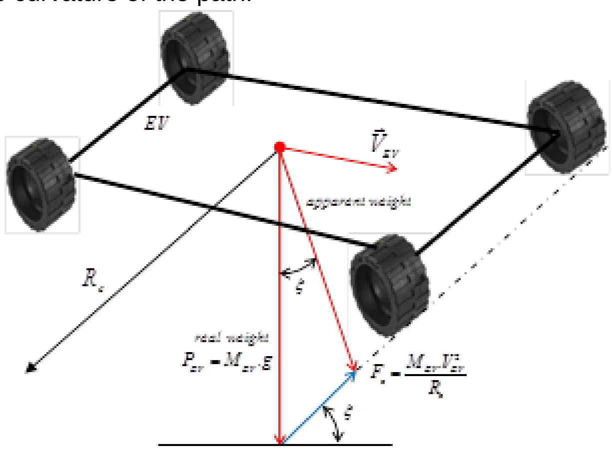

Fig.30. *Forces applied in a curved path to anelectric vehicle*

By referring to the previous figure, we write:

$$tg(\xi) = \frac{V_{EV}^2}{R_c.g} \qquad (81)$$

Thus, the total resultant force *Fr* applied to a moving vehicle in the different types of roads is given by the relation:

$$F_r = F_{rap} + F_{rrol} + F_{rst} + F_c \qquad (82)$$

Then:

$$F_r = \frac{1}{2}.\rho_{VE}.S.C_x.V_{VE}^2 + M_{VE}.g.(k_{1rrol} + k_{2rrol}.V_{VE}^2) + P_{VE}.sin(\delta_p) + \frac{M_{EV}.V_{EV}^2}{R_c} \qquad (83)$$

Finally:

$$F_r = P_{VE}.k_{1rrol} + P_{VE}.sin(\delta_p) + (\frac{1}{2}.\rho_{VE}.S.C_x + P_{VE}.k_{2rrol} + \frac{M_{EV}}{R_c}).V_{VE}^2 \qquad (84)$$

This total resistive force can be expressed as follows:

$$F_r = F_{r0} + F_{r1}(\delta_p) + F_{r2}.(V_{VE}^2) \qquad (85)$$

Where:

$$\begin{cases} F_{r0} = P_{VE}.k_{1rrol} \\ F_{r1}(\delta_p) = P_{VE}.sin(\delta_p) \\ F_{r2}.(V_{VE}^2) = (\frac{1}{2}.\rho_{VE}.S.C_x + P_{VE}.k_{2rrol} + \frac{M_{EV}}{R_c}).V_{VE}^2 \end{cases} \qquad (86)$$

Therefore, we write the total resistant force opposed to the movement of the vehicle is three-dimensional:

$$F_r = f_{VE}(P_{VE}, \delta_p, V_{VE}^2) \qquad (87)$$

The dynamics of the electric vehicle brought on the motor shaft then becomes:

$$\begin{cases} \frac{d\Omega_m}{dt} = \frac{T_{em} - r.R_w.f_{VE}(P_{VE},\delta_p,V_{VE}^2) - D_{tm}.\Omega_m}{J_{tm}} \\ \frac{d\theta_m}{dt} = \Omega_m \end{cases} \qquad (88)$$

Then:

$$\begin{cases} \frac{d\Omega_m}{dt} = \frac{T_{em} - r.R_w.f_{VE}(P_{VE},\delta_p,V_{VE}^2) - D_{tm}.\Omega_m}{J_{tm}} \\ \frac{d\theta_m}{dt} = \frac{1}{r.R_w}.V_{VE} \end{cases} \qquad (89)$$

Taking into account the link between the linear speed of the electric vehicle V_{VE} and that of the wheels Ω_w:

$$\begin{cases} V_{VE} = R_w.\Omega_w \\ \Omega_w = r.\Omega_m \end{cases} \qquad (90)$$

We obtain:

$$F_{r2}.(\Omega_m^2) = r^2.R_w^2.(\frac{1}{2}.\rho_{VE}.S.C_x + P_{VE}.k_{2rrol} + \frac{M_{EV}}{R_c}).\Omega_m^2 \qquad (91)$$

15 Simulations and Results

We simulated the behavior of an electric vehicle with the following parameters:

$\rho_{VE} = 1.3 Kg.m^{-3}$ The density of the vehicle,

$S = 1.2 m^2$ The surface taken to the wind,

$C_x = 0.29$ Coefficient of penetration into air,

V_{VE} Electric vehicle speed.

$M_{VE} = 1400 Kg$ The mass of the vehicle,

$g = 9.81 m.s^{-2}$ The acceleration of gravity,

$k_{1rrol} = 12{,}5.10^{-3}, k_{2rrol} = 32{,}4.10^{-6}$ Coefficients of rolling resistance.
$r = 0.92$ the speed reduction ratio.
$R_w = 0.3m$ The radius of the EV wheel.

The parameters of the PMSM motor are:
stator resistance: $R_s = 0.4578\Omega$, d-axis inductance: $L_d = 0.00334H$, q-axis inductance: $L_q = 0.00334H$,flux: $\phi_f = 0.171 weber$,inertia: $J_m = 0.01469 Kg.m^2$, pair poles: $p = 4$, nominal torque: $T_{emn} = 20 N.m$, friction: $D_m = 0.00334 N.m$ We simulated the case where from the instant $t = 1.2s$ up to $t = 5s$ the electric vehicle attacks a slope of $\delta_p = 30^0$.

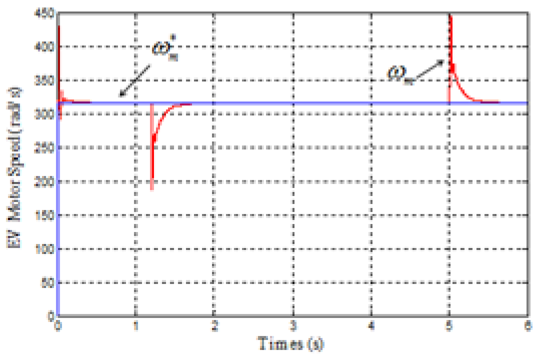

Fig.31. *rotational speed of the PMSM motor* ω_m

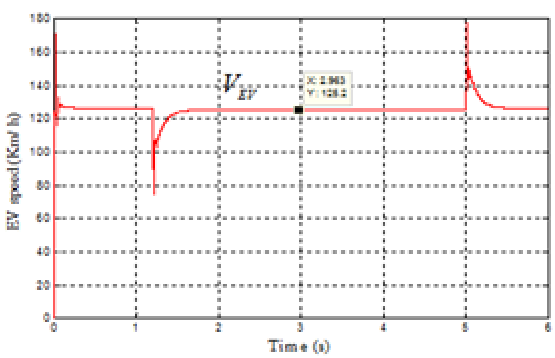

Fig.32. *Time evolution of electric vehicle speed*

Once the electric vehicle EV starts the rise of the slope, the associated regulators act so that the rotational speed of the PMSM motor ω_m catches up to its reference value ω_m^* in an extremely short time. Therefore, the vehicle speed V_{EV} remains constant during the climb. This demonstrates the robustness of integrated fuzzy control loops.

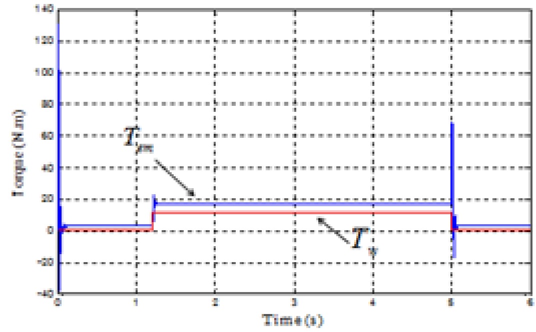

Fig.33. *Time evolution of the electromagnetique and resistive torques*

We simulated the case where from the instant $t = 1.2s$ up to $t = 5s$ the electric vehicle attacks a slope of 8%.

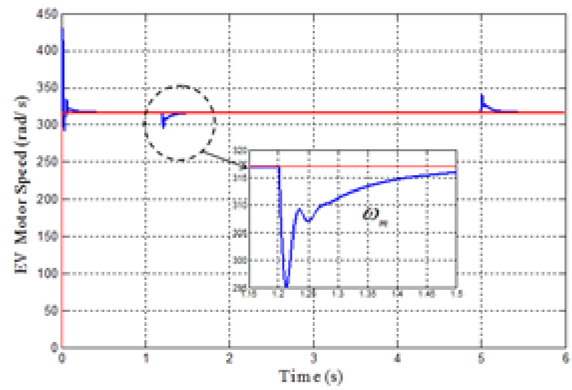

Fig.34.Time evolution of ω_m

During the rise in a slope the variations in the speed of the PMSM are similarly insignificant.

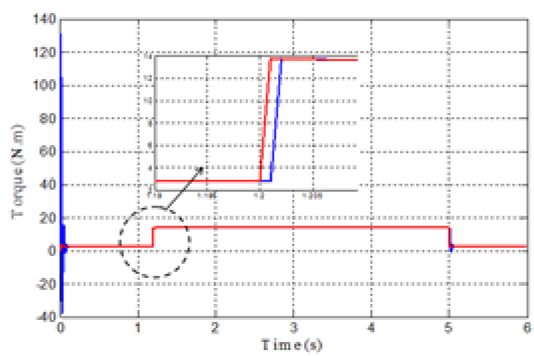

Fig.35.*Torque evolution during the rise in a slope of* 8%

The electromagnetic torque *Tem* perfectly compensates for the resistive torque *Tw* resulting essentially from the sloping rise δ_p.

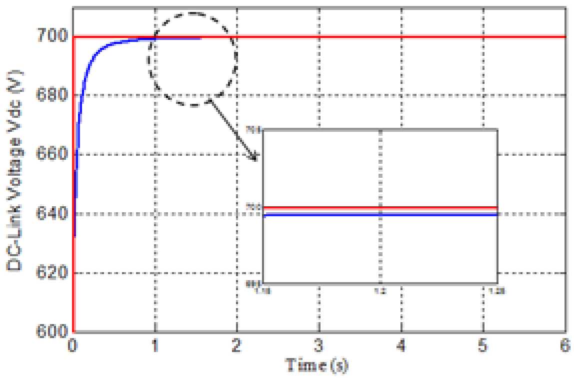

Fig.36. *Time evolution of the DC link voltage* V_{dc}

The level of the DC bus voltage V_{dc} remains insensitive to the torque rise of the electric vehicle, which proves that the control strategies adopted have perfectly isolated the engine power system from any abrupt change in the EV vehicle operator mode.

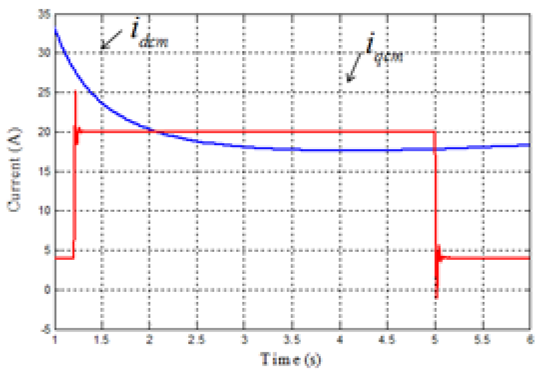

Fig.37. *Time evolution of current*

The q-axis component of the current i_{qcm} supplied by the converter C_{PMSM} acts in a notable manner to compensate for the resistive torque.This results from the fact that this component is the most weighted $\phi_{dm}.i_{qcm}$ in the expression of the electromagnetic torque T_{em}. We simulated the descent of the electric vehicle with a negative slope of -8%.

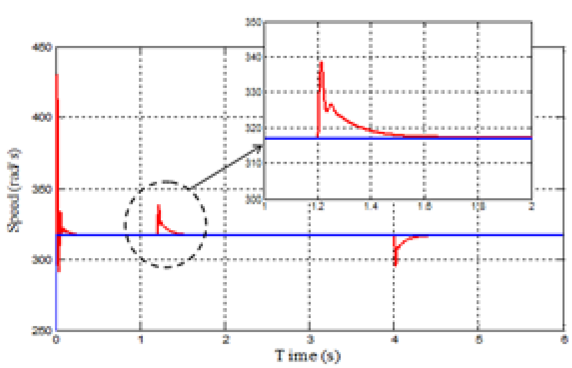

Fig.38. *Time evolution of* ω_m *during a negative slope* -8%

We notice that when the vehicle picks up speed V_{EV} at the beginning of the descent, the regulators engage a braking strategy and we notice that the speed regains its reference value. On the other hand, we observe the engagement of a regenerative braking strategy because the torque becomes negative and the motor returns electrical energy to the battery.

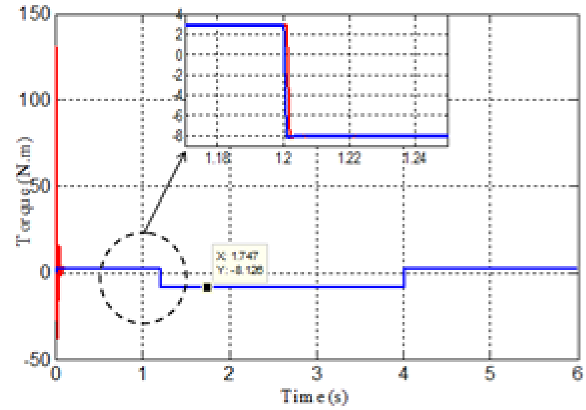

Fig.39. *Time evolution of* T_{em} *and* T_w *during a negative slope* -8%

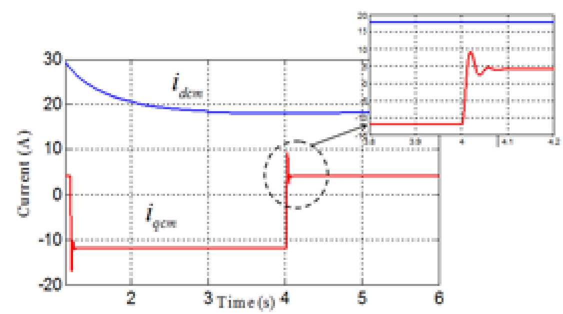

Fig.40. *Time evolution of* i_{dcm} *and* i_{qcm} *during a negative slope* -8%

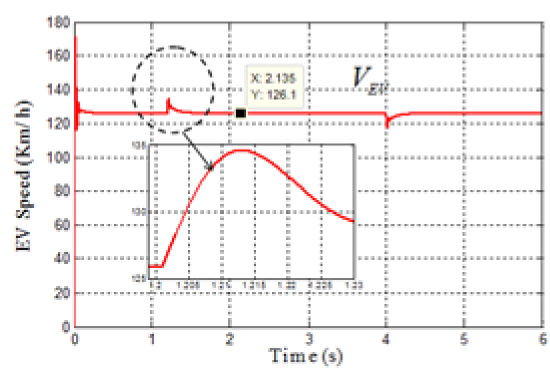

Fig.41. *Time evolution of* V_{EV} *during a negative slope* -8%

Similarly, during the descent into a ramp, the fuzzy control strategies act in such a way as to attenuate the excesses of certain state variables. We simulated the behavior of the electric vehicle the moment it takes a turn, that is to say when it is subjected to the centrifugal force F_c which pushes it towards the outside of the curve.

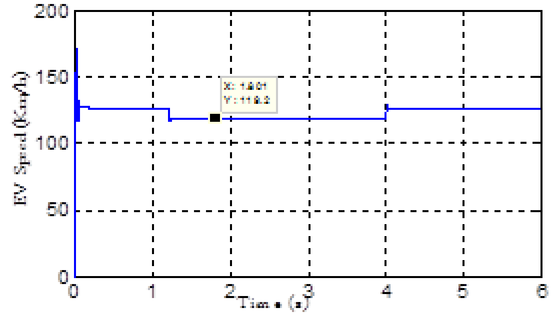

Fig.42. *Time evolution of* V_{EV} *during a curved path with a curvative radius* $R_c = 100m$

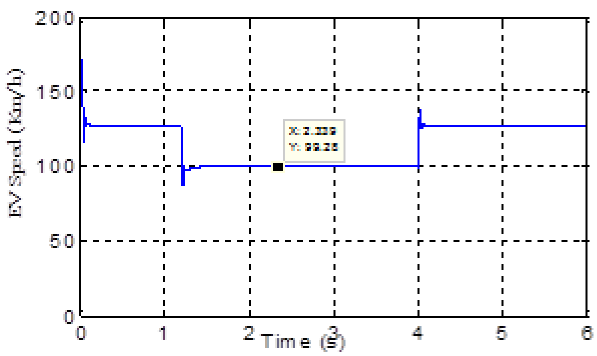

Figure.43. *Time evolution of* V_{EV} *during a curved path with a curvative radius* $R_c = 10m$

During the turning, the control strategies fuzz act to reduce the excess speed and this by an evaluation of new references ensuring an extreme degree of safety.

16 Conclusion

In this work, we are interested in the implementation of intelligent strategies based on fuzzy controllers to ensure optimal operation of an electric vehicle.we can say that the design and optimization of the traction chain of an electric vehicle is a multidisciplinary problem that must take into consideration, at a minimum, batteries, mechanical transmission and electromagnetic powered electronics. The search for a minimal cost is added to the scientific and technological difficulties. The future electric vehicle must be able, with appropriate control, to use the energy stored in the batteries in order to sustain the electricity network during periods of peak consumption or in case of emergency (shutdown of a production plant) . The energy stored in the battery of the vehicle could also supply the electrical requirements of the dwelling. This technology requires that the charger embedded in the vehicle as well as the interface between the vehicle and the electrical network are bidirectional. The results obtained are extremely encouraging and prove that the more we refine the electromagnetic model of the electric vehicle the more we obtain a favorable ground for a better implementation of the strategies of control especially the fuzzy strategies.

References

[1] CONTROL SYSTEMS FOR HIGH PERFORMANCE ELECTRIC CARS
PEDRET Paula, WEBB Jonathan, , BAYONA Guillermo, MOURE Christophe, BOLTSHAUSER Sandro
Volume 6 - Issue 1 - Pages 88-94.

[2] DESIGN CONSIDERATIONS FOR FAST AC BATTERY CHARGERS
BERTOLUZZO Manuele, BUJA Giuseppe, PEDE GIOVANNI
Volume 6 - Issue 1 - Pages 147-154, World Electric Vehicle Journal Vol. 6 - ISSN 2032-6653 - © 2013 WEVA.

[3] M. ISMAIL, M. Mustafa HASSAN "Load Frequency Control Adaptation Using Artificial Intelligent Techniques for One and Two Different Areas Power System" International Journal of Control, Automation and Systems IJCAS, Vol. 1, NO. 1, january 2012, p12-p23.

[4] A. M.A.Haidar,A. Mohamed and A. Hussain,"Vulnerability control of large scale interconnected power system using neuro-fuzzy load shedding approach",Expert Systems With Applicatons, Elsevier 37.pp. 3171-3176, 2010.

[5] MOTOR-GENERATOR CONTROL TO IMPROVE SHIFT QUALITY FOR A DUAL MODE POWER SPLIT TRANSMISSION
HONG Sungwha, CHOI Woulsun, AHN Sunghyun, LEE Geontae, SON Hanho, KIM Yongjoo, KIM Hyunsoo
Volume 6 - Issue 2 - Pages 245-250, World Electric Vehicle Journal Vol. 6 - ISSN 2032-6653 - © 2013 WEVA .

[6] Alireza Alfi, "Hybrid state-feedback sliding-mode controller design using fuzzy logic for four-wheel-steering vehicles ", Vehicle System Dynamics, vol. 47, Issue. 3, pp. 265-284, 2009.

[7] Alireza Alfi, "Swarm optimization tuned Mamdani fuzzy controller for diabetes delayed model ", Turkish Journal of Electrical Engineering and Computer Sciences, vol. 21, pp. 2110-2126, 2013.

[8] Alireza Alfi, "Optimal design of type-2 fuzzy controller using particle swarm optimization for HVAC systems", Automatika-Journal for Control, Measurement, Electronics, Computing and Communications, vol. 55, vol. 1, pp. 69-78, 2014.

[9] D. Nazari, M. Abadi, M. H. Khooban, A. Alfi, M. Siahi "Design of optimal self-regulation Mamdani-type fuzzy inference controller for type 1 diabetes mellitus", Arabian Journal for Science and Engineering, vol. 39, pp. 977-986, 2014.

[10] M. H. Khooban, A. Alfi and Abadi, "Control of a class of nonlinear uncertain chaotic systems via an optimal type-2 fuzzy PID controller", IET Science, Measurement & Tecnology, vol. 7, no. 1, pp. 50-58, 2013.

[11] M. Hassan Khooban, Alireza Alfi, Davood Nazari and Maryam Abadi, "Teaching learning based optimal interval type-2 fuzzy PID controller design: A nonholonomic wheeled mobile robots", Robotica, vol. 31, no. 7, pp. 1059-1071, 2013.

[12] A. Alfi, A. Akbarzadeh Kalat and M. Hassan Khooban , "Adaptive fuzzy sliding mode control for synchronization of uncertain non-identical chaotic systems using bacterial foraging optimization" Journal of Intelligent & Fuzzy Systems 26(2014) 2567-2576, DOI: 10.3233/IFS-130928 IOS Press.

[13] Oscar Castillo, Patricia Melin, Jausz Kacprzyk, Wiltold Pedrycz," Type 2 Fuzzy Logic : Theory and Applications", IEEE International Conference on Granular Computing, 2007.

[14] IMPACT OF ELECTROMOBILITY ON AUTOMOTIVE ARCHITECTURES
LUCCARELLI Martin, RUSSO SPENA Pasquale, MATT Dominik
Volume 6 - Issue 1 - Pages 1-8, World Electric Vehicle Journal Vol. 6 - ISSN 2032-6653 - © 2013 WEVA .

[15] H. Jouini, K. Jemaï, and S. Chebbi,"Voltage Stability Control of Electrical Network using Intelligent Load Shedding Strategy based on Fuzzy Logic", Hindawi Publishing Corporation, Mathematical Problems in Engineering, Volume 2010, Article ID 341257, 17 pages.

[16] K. Jemaï, " New Fuzzy Approach for Modeling Random Disturbances", Journal of Control Science and Engineering, Volume 2, Number 1, P 16-27, February 2014 (Serial Number 2).

[17] A. Ouederni, K. Jemaï, H. Trabelsi, "Modelling and Control of a PMSG-Based Variable Speed Wind Turbine under Unbalanced Conditions", International Journal of Research and Reviews in Electrical and Computer Engineering (IJRRECE), Vol. 2, No. 1, March 2012, ISSN: 2046-5149.

[18] IMPLEMENTING ELECTRIC VEHICLES IN URBAN DISTRIBUTION: A DISCRETE EVENT SIMULATION
LEBEAU Philippe, MACHARIS Cathy, VAN MIERLO Joeri, MAES Guillaume
Volume 6 - Issue 1 - Pages 38-47, World Electric Vehicle Journal Vol. 6 - ISSN 2032-6653 - © 2013 WEVA.